# An expanded palette of bright and photostable organellar $Ca^{2+}$ sensors

Agathe Moret, Helen Farrants, Ruolin Fan, Kelsey Zingg, Christine E. Gee, Thomas G. Oertner, Vidhya Rangaraju, Eric R. Schreiter, Jaime de Juan-Sanz*

*1. Paris Brain Institute (ICM). Sorbonne University, Inserm, CNRS, APHP, Hôpital de la Pitié Salpêtrière, Paris 75013, France.*
*2. Howard Hughes Medical Institute, Janelia Research Campus, Ashburn, United States.*
*3. Max Planck Florida Institute for Neuroscience, Jupiter, Florida, 33458, USA.*
*4. Institute for Synaptic Physiology, Center for Molecular Neurobiology (ZMNH), University Medical Center Hamburg-Eppendorf, Hamburg, Germany*
**To whom correspondence should be addressed.*

## Abstract

The use of fluorescent sensors for functional imaging has revolutionized the study of organellar $Ca^{2+}$ signaling. However, understanding the dynamic interplay between intracellular $Ca^{2+}$ sinks and sources requires bright, photostable and multiplexed measurements in each signaling compartment of interest to dissect the origins and destinations of $Ca^{2+}$ fluxes. We introduce a new toolkit of chemigenetic indicators based on HaloCaMP, optimized to report $Ca^{2+}$ dynamics in the endoplasmic reticulum (ER) and mitochondria of mammalian cells and neurons. Both ER-HaloCaMP and Mito-HaloCaMP present high brightness and responsiveness, and the use of different HaloTag ligands enables tunable red and far-red emission when quantifying organelle $Ca^{2+}$ dynamics, expanding significantly multiplexing capacities of $Ca^{2+}$ signaling. The improved brightness of ER-HaloCaMP using either red or far-red HaloTag ligands enabled measuring ER $Ca^{2+}$ fluxes in axons of neurons, in which the ER is formed by a tiny tubule of 30-60 nanometers of diameter that impeded measurements with previous red ER $Ca^{2+}$ sensors. When measuring ER $Ca^{2+}$ fluxes in activated neuronal dendritic spines of cultured neurons, ER-HaloCaMP presented increased photostability compared to the gold-standard ER $Ca^{2+}$ sensor in the field, ER-GCaMP6-210, while presenting the same responsiveness. On the other hand, Mito-HaloCaMP presented higher responsiveness than current red sensors, and enabled the first measurements of mitochondrial $Ca^{2+}$ signaling in far-red in cell lines and primary neurons. As a proof-of-concept, we used 3-plex multiplexing to quantify interorganellar $Ca^{2+}$ signaling. We show that effective transfer of $Ca^{2+}$ from the ER to mitochondria depends on the ER releasing a critical amount of $Ca^{2+}$. When this threshold is not met, the mobilized $Ca^{2+}$ is diverted to the cytosol instead. Our new toolkit provides an expanded palette of bright, photostable and responsive organellar $Ca^{2+}$ sensors, which will facilitate future studies of intracellular $Ca^{2+}$ signaling.

## Introduction

The ability of cells to generate transient $Ca^{2+}$ fluctuations in subcellular locales is fundamental for controlling essential cellular processes such as gene expression, cell metabolism or neuronal communication[1,2]. Organelles such as mitochondria or the endoplasmic reticulum (ER) can function within cells as sinks or sources of $Ca^{2+}$ and modulate $Ca^{2+}$ dynamics across cellular compartments with

temporal and spatial precision, shaping cell physiology[3,4]. In non-excitable cells, $Ca^{2+}$ transfer between the ER and mitochondria accelerates mitochondrial metabolism to fuel energy-intensive tasks[5]. While the role of ER-mitochondria $Ca^{2+}$ transfer in excitable cells is less understood, its dysfunction is heavily associated with pathological states, contributing to a wide array of diseases that affect different cell types and tissues[3,6–8]. Not surprisingly, owing to the critical role of ER and mitochondrial $Ca^{2+}$ signaling in both physiological and pathological processes, their investigation has garnered significant attention over the past several decades[2,9].

While for many years insights into organellar $Ca^{2+}$ functions were primarily based on indirect cytosolic $Ca^{2+}$ measurements coupled with organelle-specific manipulations, recent advancements now enable measuring $Ca^{2+}$ directly in ER or mitochondria using genetically encoded sensors (GECIs)[10–15]. These tools have enabled precise quantification of $Ca^{2+}$ dynamics in these organelles in live cells and intact tissue. Among the series of GECIs developed for mitochondria and the ER, those based on green fluorescent protein-based sensors such as GCaMP have stood up due to their high sensitivity in detecting $Ca^{2+}$ dynamics in both ER and mitochondria[10,11,13,16–19]. However, GFP-based GECIs have inherent limitations. First, their excitation spectrum overlaps with other commonly used fluorescent proteins and optogenetic tools, complicating multicolor imaging needed for dissecting complex cellular processes; second, the higher background autofluorescence in biological tissues can reduce signal-to-noise ratio, making it difficult to accurately detect calcium dynamics in small organellar structures, like the single small ER tubule present in axons of neurons; third, GFP-based GECIs also typically suffer from lower photostability, leading to rapid photobleaching that limits prolonged experiments. These limitations suggest that red-shifted GECIs could provide a reliable imaging alternative in these cellular compartments. However, despite recent advances, the currently available red-shifted GECIs designed for ER and mitochondrial Ca $Ca^{2+}$ imaging exhibit significant limitations, either presenting excessively high affinity[14] or showing poor responsiveness or dynamic range[10,12], thereby constraining their usability. Additionally, the lack of far-red sensors specific to these organelles has further limited simultaneous multi-wavelength imaging of organellar and cytosolic $Ca^{2+}$ dynamics, along with other key physiological markers, limiting our detailed understanding of $Ca^{2+}$ fluxes and their relevance for cellular physiology in health and disease.

These limitations highlight the need for innovative approaches that overcome the shortcomings of current organellar GECIs. In this work, we present a new suite of chemigenetic indicators derived from HaloCaMP, a genetically encoded $Ca^{2+}$ sensor whose fluorescence is provided by HaloTag Ligands (JF-HTL), permeable rhodamine dyes of the color of choice[20]. We generated novel HaloCaMP sensors, tailored specifically for precise $Ca^{2+}$ measurements in the ER and mitochondria, which we name ER-HaloCaMP and Mito-HaloCaMP. These sensors provide a significant improvement in organelle-targeted $Ca^{2+}$ imaging by combining robust responsiveness together with the enhanced brightness and great photostability provided by the rhodamine dyes. Along with these advantages, the indicators feature tunable red and far-red emission, enabling compatibility with multicolor imaging without the spectral overlap or interference issues commonly associated with GFP-based sensors. We compared these new sensors to existing red-emitting GECIs and showed that they exhibit a 10-fold increase in brightness and 3-fold improved responsiveness to physiological stimuli compared to the best-performing variants for ER and mitochondrial $Ca^{2+}$ measurements. Remarkably, the responsiveness of ER-HaloCaMP reconstituted with $JF_{585}$-HTL (ER-HaloCaMP$_{585}$) in cells and neurons was indistinguishable from the gold-standard ER $Ca^{2+}$ sensor ER-GCaMP6-210[11], but its photostability and brightness-over-background were significantly improved, making it the ideal sensor for ER $Ca^{2+}$ measurements. Our work provides a new technological

framework to enable novel investigations into cellular $Ca^{2+}$ fluxes, offering new insights into the fundamental role of $Ca^{2+}$ signaling in health and disease.

# Results

### Developing a bright and highly responsive red ER $Ca^{2+}$ sensor based on HaloCaMP.

The ER contains ~2000 times more $Ca^{2+}$ than the cytosol, making it impossible to use the existing large palette of red GECIs developed over the years for cytosolic $Ca^{2+}$ measurements. To overcome this issue, previous efforts have screened for mutants of GECIs to identify low affinity variants whose $K_D$ is close to the resting $Ca^{2+}$ levels found in the ER yet maintain a responsiveness close to the original sensor. The first efforts to obtain red-shifted ER $Ca^{2+}$ sensors generated LAR-GECOs, which preserved good dynamic range yet their affinity for $Ca^{2+}$ was not lowered enough to match ER $Ca^{2+}$ levels, limiting their usability[14]. Alternative approaches generated R-CEPIAer, which presented low affinity yet its responsiveness remained limited compared to the standards of green ER GECIs[10]. To circumvent these issues and expand the wavelengths of emission of ER $Ca^{2+}$ sensors beyond red, we first generated a series of HaloCaMP variants harboring combinations of mutations in key $Ca^{2+}$-coordinating sites to lower their affinity and evaluate their responsiveness (Fig. 1A; Supp. Fig. S1A). Using purified sensors conjugated *in vitro* with $JF_{585}$-HTL, we performed $Ca^{2+}$ titrations and identified a variant that presented both high dynamic range (~15 $\Delta F/F$) and low affinity (Kd = 86μM), which we named Low Affinity (LA)-$HaloCaMP1a_{585}$ (Fig. 1B). The general properties of this low affinity variant did not significantly change when titrations were performed at 37°C, supporting their usability for live cell experiments (Supp. Fig. S1B). As a control, we confirmed that micromolar/millimolar increases in $Ca^{2+}$ did not cause any increase in $HaloTag_{585}$ fluorescence, indicating that $JF_{585}$-HTL itself is not responsive to high $Ca^{2+}$ (Fig. 1B).

We next targeted LA-HaloCaMP1a fused to mTagBFP2 to the lumen of the ER by flanking it with a modified calreticulin signal peptide and a KDEL retention motif, as successfully used for ER-GCaMP6[11]. This construct was efficiently expressed in the ER of HeLa cells, and we confirmed that $JF_{585}$-HTL successfully traversed both the plasma and ER membranes, demonstrating that conjugation between sensor and dye in the ER is possible (Fig. 1C). We performed *in-cell* $Ca^{2+}$ titrations in permeabilized HeLa cells and confirmed that ER-HaloCaMP presents a low affinity of 115 μM (Supp. Fig S1C), slightly lower than purified protein. Such a shift between purified and *in-cell* sensor properties is expected and it has been already observed for ER-GCaMP6 variants[21]. Given the higher dynamic range of ER-HaloCaMP and its better suited affinity for ER $Ca^{2+}$ than LAR-GECO and R-CEPIAer in purified protein (Fig. 1D), we next sought to compare its responsiveness against these sensors under common ER $Ca^{2+}$ perturbations, such as thapsigargin-induced ER $Ca^{2+}$ depletion. Quantifying responses in both HeLa cells and somas of primary cortical neurons, we observed that although LAR-GECO and R-CEPIAer responded to thapsigargin as previously reported[10,14,22], ER-$HaloCaMP_{585}$ exhibited a significantly larger response in both cell types (Fig. 1E). These results indicate that ER-$HaloCaMP_{585}$ provides a significant improvement in red ER $Ca^{2+}$ imaging over previous technologies.

We next compared the brightness of ER-$HaloCaMP_{585}$ against previous red ER $Ca^{2+}$ sensors. While the ER is abundant and easily detectable when measured in bulk within a cell, the small diameter of individual ER tubules, approximately 60 nm, can hinder ER $Ca^{2+}$ detection in certain subcellular locales. For example, this problem becomes even more apparent when studying neuronal projections, which can contain up to a single narrow ER tubule in the case of axons[23,24] or dendritic spines[24,25]. We thus reasoned

that sensors presenting increased brightness should provide the field with better tools to study ER $Ca^{2+}$ in subcellular compartments. Using identical illumination and detection conditions, we compared the relative brightness of LAR-GECO, R-CEPIAer and ER-HaloCaMP$_{585}$ and found that ER-HaloCaMP$_{585}$ exhibited about a 100-fold enhancement in brightness in HeLa cells and approximately a 20-fold enhancement in somas of primary neurons (Fig. 1F, G). Next, we investigated the ability of these sensors to detect ER fluorescence within the single, narrow ER tubules of axons, a task that represents a significant challenge in ER $Ca^{2+}$ imaging. This comparison provided a substantial improvement over previous technologies, as neither LAR-GECO nor R-CEPIAer enabled axonal ER detection in any neuron presenting somatic ER labeling, whereas ER-HaloCaMP$_{585}$ allowed us to identify it clearly in over 50% of the transfected neurons (Fig. 1H; see Materials and Methods).

**ER-HaloCaMP enables bright and photostable ER $Ca^{2+}$ measurements in compartments with low ER content.**

As ER-HaloCaMP$_{585}$ is the main red ER $Ca^{2+}$ sensor visible in axons of neurons, we sought to evaluate its responsiveness in such a small compartment. Axonal ER uptakes $Ca^{2+}$ from the cytosol during neurotransmission via sarcoplasmic/endoplasmic reticulum $Ca^{2+}$-ATPases (SERCAs)[11,26,27]. We electrically stimulated primary cortical neurons to mimic physiological firing paradigms of neurons *in vivo*, such as firing at 20 Hz for 1s[28], and quantified axonal ER $Ca^{2+}$ dynamics using ER-HaloCaMP$_{585}$. We observed robust activity-driven ER $Ca^{2+}$ uptake, which was completely silenced when inhibiting SERCA pumps using Thapsigargin, confirming the specificity of the measurements (Fig. 2A,B). Since other red ER $Ca^{2+}$ sensors appeared insufficiently visible in axons, we compared the performance of ER-HaloCaMP$_{585}$ with the current gold standard ER $Ca^{2+}$ sensor, the GFP-based ER-GCaMP6-210[11]. Remarkably, ER-HaloCaMP$_{585}$ exhibited uptake responses comparable to those of ER-GCaMP6-210, demonstrating its high efficacy in measuring ER $Ca^{2+}$ dynamics within small ER volumes (Fig. 2C,D).

To examine whether ER-HaloCaMP$_{585}$ could also accurately detect physiological ER $Ca^{2+}$ release (causing a decrease in signal) and not only uptake (increase in signal), we assessed its responsiveness in neuronal dendrites, another subcellular localization containing limited amounts of ER. During excitatory neurotransmission, dendrites receive extracellular glutamate inputs from other neurons, which drive $Ca^{2+}$ entry from the extracellular space and cause $Ca^{2+}$-induced $Ca^{2+}$ release from dendritic ER[17,29]. To study this process we generated localized extracellular glutamate increases in the vicinity of single spines of dendrites using glutamate uncaging and examined ER $Ca^{2+}$ responses using ER-HaloCaMP$_{585}$. Our experiments revealed that ER-HaloCaMP$_{585}$ detected single-pulse uncaging ER $Ca^{2+}$ release events with a high signal-to-noise ratio, and the magnitude of these events was indistinguishable from those obtained with ER-GCaMP6-210 (Fig. 2E-G). Moreover, when comparing the photostability of prolonged measurements of ER $Ca^{2+}$ release, we found that signals of ER-HaloCaMP$_{585}$ robustly recovered to the initial baseline, while ER-GCaMP6-210 showed a loss of fluorescence after the experiment, suggesting impaired photostability (Fig. 2H). When evaluating the performance of ER-GCaMP6-210 versus ER-HaloCaMP$_{585}$, we observed that ER-GCaMP6-210 exhibited a rapid decrease in fluorescence immediately after imaging began in both dendrites and axons, which then quickly settled into a new steady-state baseline. This phenomenon has been previously observed[29], however its origin remains unclear, it could be due to selective photobleaching or photoswitching of distinct populations of ER-GCaMP molecules when blue light is shined into samples. ER-HaloCaMP$_{585}$ in contrast maintained a consistently stable and bright fluorescence signal throughout the imaging period in both axons and dendrites, showing improved

photostability when detecting ER $Ca^{2+}$ dynamics. These findings suggest that ER-HaloCaMP$_{585}$ is ideally suited for quantifying ER $Ca^{2+}$ dynamics in subcellular regions with low ER content.

**ER-HaloCaMP fluorescence is tunable and enables far-red ER $Ca^{2+}$ measurements**

We next evaluated the usability of ER-HaloCaMP conjugated with JF$_{635}$-HTL (ER-HaloCaMP$_{635}$) for measuring ER $Ca^{2+}$ levels in the far-red spectrum, which, to our knowledge, has not yet been possible. Conjugation with JF$_{635}$-HTL instead of JF$_{585}$-HTL caused a shift in the $Ca^{2+}$ affinity of ER-HaloCaMP, increasing its affinity by approximately threefold (not shown). When imaged in HeLa cells, ER-HaloCaMP$_{635}$ generated a clear pattern of ER labeling and, upon thapsigargin addition, it successfully detected dynamic ER $Ca^{2+}$ changes in the far red channel, confirming its usability as ER $Ca^{2+}$ sensor (Fig. 3A). This strategy provides, to our knowledge, the first system for far red ER $Ca^{2+}$ imaging in live cells. Given the lack of other far red ER $Ca^{2+}$ sensors for direct comparison, we evaluated ER-HaloCaMP$_{635}$ by comparing its $\Delta F/F$ changes to those of ER-GCaMP6-210. The results showed that the changes detected by ER-HaloCaMP$_{635}$ were approximately in the same range as those observed with ER-GCaMP6-210 (Fig. 3B,C). This supports the versatility of ER-HaloCaMP in capturing ER $Ca^{2+}$ dynamics in live cells across different fluorescence colors. We then investigated whether ER-HaloCaMP$_{635}$ could be used to visualize ER fluorescence within the narrow ER tubules of axons and monitor ER $Ca^{2+}$ dynamics. We first confirmed that ER-HaloCaMP$_{635}$ also enabled successful detection of axonal ER. Then, we electrically stimulated neurons and observed robust axonal ER $Ca^{2+}$ uptake. As control, signals were completely silenced by Thapsigargin, confirming the specificity of the measurements (Fig. 3E). Benchmarking against ER-GCaMP6-210 showed that ER-HaloCaMP$_{635}$ is not as responsive as ER-HaloCaMP$_{585}$, yet it generated consistent responses during electrical stimulation (Fig. 3F). These results show, to our knowledge, the first measurements of ER $Ca^{2+}$ dynamics in the far red channel, which are possible even in subcellular locales presenting very low ER content.

**Developing a responsive and tunable red/far-red mitochondrial $Ca^{2+}$ sensor based on HaloCaMP.**

Given the great characteristics of ER-HaloCaMP, we extended our strategy to develop mitochondrial $Ca^{2+}$ sensors based on HaloCaMPs. Mitochondrial $Ca^{2+}$ uptake occurs dynamically in cells and it is essential for cellular physiology, as it adjusts energy production, modulates metabolic pathways and influences cell survival and apoptosis[9]. Resting free $Ca^{2+}$ in mitochondria is higher than cytosolic $Ca^{2+}$, yet still remains in the hundreds of nanomolar range[13,30–32]. Previous studies have shown that low-affinity mitochondrial $Ca^{2+}$ sensors exhibit inadequate responses to capture physiological stimuli in HeLa cells[10] and neurons[33]. In contrast, adapting sensors originally developed for cytosolic $Ca^{2+}$ measurements has yielded robust mitochondrial responses[13,33]. We targeted HaloCaMP1a to mitochondria by using tandem mitochondrial targeting sequences from cyclooxygenase 8 and fused it with mTagBFP2 to create Mito-HaloCaMP (Fig. 4A). We expressed Mito-HaloCaMP in HeLa cells and conjugated it with JF$_{585}$-HTL, which generated a bright mitochondrial pattern in HeLa cells that upon histamine addition reported a robust change in mitochondrial $Ca^{2+}$ (Fig. 4B). To assess the efficacy of Mito-HaloCaMP$_{585}$, we conducted comparative analyses against Mito$^{4x}$-jRCaMP1b[13,34] by measuring their respective $\Delta F/F$ responses and brightness under identical conditions. Our results demonstrated that Mito-HaloCaMP$_{585}$ not only exhibited significantly larger $\Delta F/F$ changes but was also significantly brighter, indicating enhanced sensitivity and improved signal strength for monitoring mitochondrial $Ca^{2+}$ dynamics in HeLa cells (Fig. 4B-D).

In non-excitable cells and neuronal somata, mitochondria are easily detectable and form networks of elongated structures. However, in axons their morphology is significantly reduced and they appear as small rounded structures averaging approximately 1 μm in length, thereby making their detection significantly more challenging. We next used Mito-HaloCaMP$_{585}$ to identify axonal mitochondria and electrically stimulated neurons to fire 20AP at 20Hz as before (Fig. 4E). During neuronal firing, we observed that Mito-HaloCaMP$_{585}$ exhibited robust mitochondrial $Ca^{2+}$ responses, generating fluorescence changes that were 3.5-fold greater than those obtained with Mito-jRCaMP1b under identical conditions (Fig. 4F). Similarly, when stimulating neurons with 100AP fired at 100Hz, Mito-HaloCaMP$_{585}$ still reported significantly larger changes (Fig. 4F,G). These findings indicate that Mito-HaloCaMP$_{585}$ represents a significant advancement in mitochondrial $Ca^{2+}$ imaging technology, providing a brighter and more responsive tool for red mitochondrial $Ca^{2+}$ measurements.

We next evaluated the usability of Mito-HaloCaMP conjugated with JF$_{635}$-HTL (Mito-HaloCaMP$_{635}$) for measuring mitochondrial $Ca^{2+}$ dynamics in the far-red spectrum, which, to our knowledge, has not yet been possible (Fig. 4H). We reasoned that the ability of measuring organellar $Ca^{2+}$ handling in the far red spectrum should enable quantifying $Ca^{2+}$ dynamics in the different subcellular compartments involved in ER-mitochondria $Ca^{2+}$ transfer, enabling the detection of $Ca^{2+}$ in three independent subcellular locales. Using first ATP as a stimulus to drive ER $Ca^{2+}$ release, we simultaneously quantified $Ca^{2+}$ dynamics in ER, cytosol and mitochondria of HeLa cells (Fig. 4I), and observed that the amplitude of both mitochondrial and ER $Ca^{2+}$ correlated with the amplitude of cytosolic $Ca^{2+}$ increases (Fig. 4J). Although endoplasmic reticulum and cytosolic $Ca^{2+}$ dynamics appeared closely correlated during ATP stimulation, the activation of both ionotropic and metabotropic ATP receptors complicates the definitive quantification of ER-to-mitochondria $Ca^{2+}$ flux, as extracellular $Ca^{2+}$ entry may also contribute to the observed signals. To assess ER–mitochondria $Ca^{2+}$ transfer, we next stimulated ER $Ca^{2+}$ release with histamine and quantified how much of the released $Ca^{2+}$ reached mitochondria versus how much remained in the cytosol. Quantitative single-cell measurements revealed that when the amount of ER-released $Ca^{2+}$ falls below a certain threshold, virtually no $Ca^{2+}$ is delivered to mitochondria, and most is detected in the cytosol. However, once this threshold is surpassed, the fraction of $Ca^{2+}$ transferred to mitochondria relative to the cytosol remains constant (Fig. 4K). This indicates that a minimal level of ER $Ca^{2+}$ release is required to trigger effective ER–mitochondria $Ca^{2+}$ coupling, after which transfer proceeds in a stable, proportionate manner (Fig. 4K). This novel strategy to monitor ER-mitochondria $Ca^{2+}$ transfer should provide a robust framework to explore the fitness of this process in different cell states in health and disease.

Lastly, we examined the capabilities of Mito-HaloCaMP$_{635}$ to detect mitochondrial $Ca^{2+}$ uptake in single mitochondria of the axon during neuronal activity (Fig. 4L). We electrically stimulated neurons to fire 20AP at 20Hz or 100AP at 100Hz as before and observed that Mito-HaloCaMP$_{635}$ exhibited robust mitochondrial $Ca^{2+}$ responses, generating fluorescence changes detectable in individual mitochondria (Fig. 4L-N). As there are no far red mitochondrial $Ca^{2+}$ sensors, we compared Mito-HaloCaMP$_{635}$ to Mito-GCaMP6f, the gold standard in the field. We found that Mito-GCaMP6f was only slightly more responsive than Mito-HaloCaMP$_{635}$ demonstrating the high sensitivity of Mito-HaloCaMP$_{635}$ in for these experiments, which should be among the most challenging mitochondrial $Ca^{2+}$ measurements in cultured cells.

# Discussion

The interplay between cytosolic and organellar $Ca^{2+}$ pools orchestrates a myriad of cellular responses essential for cellular function and survival[2,35], correspondingly, different cellular states are associated with different organellar $Ca^{2+}$ signaling[36]. However, much of our knowledge on organellar $Ca^{2+}$ signaling across fields of biology has relied on indirect approaches that inferred organellar $Ca^{2+}$ dynamics from cytosolic data or monitored luminal $Ca^{2+}$ in distinct compartments but in separate experiments[17,37–39]. While highly valuable, such methods do not enable capturing variability of organellar responses in single cells, which is often large and could be reflecting very diverse cell states, making the interpretation of averaged data complicated. For example, when studying ER-mitochondria $Ca^{2+}$ transfer, several labs in recent years have implemented dual-compartment $Ca^{2+}$ imaging to solve this problem, commonly cytosol and mitochondria or cytosol and ER[13,17,38]. However, these measurements still need separate populations of cells to study all three compartments, which may complicate interpretations when quantifying ER-mitochondria $Ca^{2+}$ transfer, perhaps contributing to the controversy of opposite results in the field.

Here we present an expanded palette of chemigenetic ER and mitochondrial $Ca^{2+}$ sensors whose fluorescence is tunable through the use of different chemical dyes emitting in different colors. Combining the robust photostability and brightness of JF-HTLs together with optimized HaloCaMP variants targeted to the ER and mitochondria, the development of ER-HaloCAMP and Mito-HaloCaMP provides the field with a two pivotal advancements: 1) Significantly improved brightness and responsiveness of ER and mitochondrial $Ca^{2+}$ measurements in the red spectrum over previous sensors; 2) First-time robust measurements of ER and mitochondrial $Ca^{2+}$ in far-red. The observed higher brightness of ER-HaloCAMP and Mito-HaloCaMP, compared to sensors such as RCEPIAer or Mito-jRCaMP1b, is consistent with measurements of HaloCaMP1a$_{635}$ at saturating $Ca^{2+}$, which show a molecular brightness about 1.7 times that of other common $Ca^{2+}$ sensors, such as GCaMP6s[20]. Such enhanced brightness of ER-HaloCaMP and Mito-HaloCaMP enables reliable $Ca^{2+}$ measurements in regions where such measurements have been historically challenging, such as in individual axonal mitochondria[13,18,19] or in the narrow ER tubules within axons[11]. Moreover, ER-HaloCaMP enabled the first red fluorescence-based measurements of $Ca^{2+}$ in axonal ER, which were previously unachievable with earlier sensors due to the small size of these structures[23]. This, together with our first measurements of ER $Ca^{2+}$ in far red, marks a significant advancement in enabling organelle-specific multiplexed calcium measurements.

Leveraging HaloTag as a scaffold for generating novel sensors has provided several novel indicators that enable measuring in different colors diverse pieces of biology. These include cytosolic $Ca^{2+}$;[20,40], voltage[41,42], ATP[43], NAD+[43], pH[44] or protein aggregation[45], among others. Indeed, the versatility of multicolor measurements together with additional properties of modified HaloTag ligands is becoming an exciting field that is providing an ever growing toolkit for the development of new sensors[46,47]. However, while several HaloTag-based strategies have provided robust multicolor cytosolic $Ca^{2+}$ sensors[20,40,48,49], suitable versions to expand the palette of organellar $Ca^{2+}$ sensors were missing. Our development of novel low affinity HaloCaMP variants provides robust ER $Ca^{2+}$ sensors and should provide the basis for developing additional organelle sensors in other locales containing large amounts of $Ca^{2+}$, such as the Golgi apparatus. JF-HTLs are fairly pH insensitive and thus it is possible that LA-HaloCaMPs may remain functional in acidic environments.

On the other hand, the development of Mito-HaloCaMP enabled us to measure mitochondrial $Ca^{2+}$ dynamics in the far-red spectrum, providing high signal-to-noise triple measurements of ER, mitochondria, and cytosolic $Ca^{2+}$ when combined with other existing sensors. This approach provided proof-of-concept data indicating that a minimal threshold of ER $Ca^{2+}$ release initiates stable ER–

mitochondria $Ca^{2+}$ coupling, after which the transfer remains proportional. These findings align with the current model in which MCU opening is controlled in an all-or-none manner by MICU family proteins that sense a critical $Ca^{2+}$ concentration in ER–mitochondria microdomains[50,51]. We find that if this threshold is not reached, ER-released $Ca^{2+}$ remains in the cytosol. These experiments reveal the importance of simultaneous measurements of different compartments when studying organellar $Ca^{2+}$ signaling.

Overall, we show that ER-HaloCAMP and Mito-HaloCaMP present improved brightness, responsiveness and flexibility, making them the preferred choice in several $Ca^{2+}$ signaling paradigms in cell lines and neurons. Thus, our expanded palette of organellar $Ca^{2+}$ sensors unlocks new possibilities for the study of organellar $Ca^{2+}$ signaling across fields, which will facilitate our understanding of organellar cell physiology in health and disease.

# Material and methods

**Lead contact.**

Further information and requests for resources and reagents may be directed to and will be fulfilled by the lead contact, Dr. Jaime de Juan-Sanz (jaime.dejuansanz@icm-institute.org).

**Resources Table.**

| Reagent or Resource | Source | Identifier |
|---|---|---|
| **Experimental models: Organisms/Strains** | | |
| HeLa cells | LGC standards | ATCC-CRM-CCL-2 |
| HEK 293T/17 | LGC standards | ATCC-CRL-11268 |
| Sprague-Dawley Rat | Charles River | Strain: Crl:CD(SD) |
| **DNA constructs** | | |
| CMV Mito-HaloCaMP | This paper | Addgene plasmid #232195 |
| CMV ER-HaloCaMP | This paper | Addgene plasmid #232198 |
| CamKII Mito-HaloCaMP | This paper | Addgene plasmid #232196 |
| CamKII ER-HaloCaMP | This paper | Addgene plasmid #232197 |
| R-CEPIAer | Suzuki et al, 2014 | Addgene plasmid #58216 |
| LAR-GECO1 | Wu et al, 2014 | Addgene plasmid #61244 |
| Mito4x-jRCaMP1b | Ashrafi et al, 2020 | Addgene plasmid #127873 |

**Molecular biology for generating the low affinity HaloCaMPs.**

Synthetic DNA oligonucleotides were purchased from Integrated DNA technologies. Q5 high fidelity DNA polymerase (New England Biolabs) was used for all PCR amplifications. Isothermal assembly reactions were performed with a NEBuilder HiFi kit (New England Biolabs). Small scale DNA isolation was performed with QIAprep Spin Miniprep Kit (Qiagen). The pRSET vector backbone was acquired from Life Technologies. Inserts and vector backbones were amplified by PCR amplification. Vector backbones and inserts were assembled by isothermal assembly with 10-30 base pair overlap, and sequence verified by Sanger sequencing (Azenta Life Sciences) or by nanopore full-plasmid sequencing (Plasmidsaurus).

**Protein expression and purification.**

For expression and purification of proteins, T7 express (New England Biolabs) were transformed with pRSET plasmids encoding for the protein of interest. The bacteria were grown in auto-induction media using the Studier method[52] with antibiotics at 30 °C for 48 h shaking at 200 rotations per minute (r.p.m.). Cell pellets were collected by centrifugation, lysed in TRIS Buffered Saline (TBS; 19.98 mM Tris, 136 mM NaCl, pH 8.0), with n-Octyl-β-D-thioglucopyranoside (5 g $L^{-1}$). Aggregations were disrupted by sonication and the lysate cleared by centrifugation. Protein purification was performed on a N-terminal poly-histidine ($His_6$) tag using HisPur Ni-NTA resin (Thermofisher Scientific), according to manufacturer's recommendations. Purified proteins were buffer exchanged into TBS using Amicon concentration filters (Merck). Protein aliquots were stored at 4 °C.

**Calcium titrations in purified protein.**

To determine the calcium affinity and cooperativity of the low affinity HaloCaMP sensors, calcium titrations were performed in a buffer system made from CaNTA and NTA prepared using the pH titration method described by Tsien and Pozzan[53] mixed in specific ratios to generate known free calcium concentrations. The free calcium concentration was calculated assuming the dissociation constant of NTA for $Ca^{2+}$ 67 µM. HaloCaMP proteins were pre-labeled with a limiting dye-HaloTag ligand (20 µM protein, 10 µM $JF_{585}$-HTL). 2 µL of the pre-labeled protein-dye conjugate was diluted into 98 µL of pre-mixed solutions of Ca-NTA in black 96-well plates. Fluorescence intensities were read on a plate reader (Tecan Spark 20M). Fluorescence intensity was measured at 26 °C and 37 °C. For HaloCaMPs with $JF_{585}$-HTL excitation was 590 nm and emission 620 nm. For GCaMPs excitation was 484 nm and emission was 510 nm. All bandwidths were set to 5 nm. Changes in fluorescence in addition of $Ca^{2+}$ were calculated in Microsoft Excel. The fluorescence (y) was plotted against the free calcium concentration (x) and a four-parameter dose-response curve (variable slope) using GraphPad Prism v10 software was fit where (a) is the value of fluorescence at the bottom of the curve, (b) is the value of fluorescence at the top of the curve, ($EC_{50}$) is the concentration of agonist that gives a response halfway between bottom and the top, and (h) is the hill or cooperative coefficient.

$$y\,(x) = a + \frac{x^h \times (b - a)}{x^h + \ {EC_{50}}^h}$$

**Animals.**

The rats of either sex used in this study to prepare primary cultures were of the Sprague-Dawley strain, Crl (SD), bred by Charles River Laboratories following the international genetic standard protocol (IGS). All experiments conducted at the Paris Brain Institute strictly followed the guidelines set by the European

Directive 2010/63/EU and the French Decree n° 2013-118 for the protection of animals used in scientific research.

**Primary rat co-culture of postnatal cortical neurons and astrocytes.**

The imaging experiments conducted on primary co-cultures of cortical neurons and astrocytes were obtained by conducting the following culture protocol: P0 to P2 rats of mixed gender were sacrificed, and their brains were dissected in a cold HBSS-FBS solution (1X HBSS + 20% Fetal Bovine Serum) to isolate the cerebral cortexes. These were then cut into small pieces for digestion and dissociation. The tissue was washed twice with 1X HBSS-FBS and 1X HBSS before being incubated in a trypsin-based digestion solution containing DNAse I (Merck, D5025) for 15 minutes at room temperature (RT). Trypsin (Merck, T1005) was neutralized with HBSS-FBS solution, followed by two washes with 1X HBSS-FBS and two with 1X HBSS. The tissue was then transferred to a dissociation solution (1X HBSS, 5.85mM $MgSO_4$) and dissociated into single cells by gentle pipetting. The cells were centrifuged at 13,000 rpm for 10 minutes at 4°C, and the pellet was resuspended in 1X HBSS solution. After a second centrifugation, the pellet was resuspended in a homemade warmed plating media consisting of MEM (Thermo Fisher Scientific, 51200038) supplemented with 20 mM Glucose (Merck, G8270), 0.1 mg/ml transferrin (Merck, 616420), 1% GlutaMAX (Thermo Fisher Scientific, 35050061), 24 µg/ml insulin (Merck, I6634), and 10% FBS (Thermo Fisher Scientific, 10082147) and 2% N-21 (Bio-techne, AR008). Finally, cells were plated in sterilized cloning cylinders (Merck, C7983; 38,000 cells per cylinder) attached to coverslips (Diameter = 25 mm, Warner Instruments, 640705) that had been pre-coated with 0.1 mg/ml poly-ornithine (Merck, P3655). After 3-4 days, the neuronal media was replaced with a homemade feeding media, similar in composition to the plating media but containing 5% FBS and 2 µM cytosine β-d-arabinofuranoside (Merck, C6645) to inhibit glial growth. The primary co-cultures of cortical neurons and astrocytes were maintained at 37°C in a humidified incubator with 95% air/5% CO2 until the imaging experiments, which were performed from DIV12 to DIV21.

For cultures used in glutamate uncaging experiments shown in Figure 2F-G, conditions were as follows: hippocampal regions were dissected in ACSF containing (in mM) 124 NaCl, 5 KCl, 1.3 $MgSO_4{:}7H_2O$, 1.25 $NaH_2PO_4{:}H_2O$, 2 $CaCl_2$, 26 $NaHCO_3$, and 11 Glucose (stored at 4°C) and stored in hibernate E buffer (BrainBits LLC, stored at 4 °C). Dissected hippocampi were dissociated using Papain Dissociation System (Worthington Biochemical Corporation, stored at 4 °C) with a modified manufacturer's protocol. Briefly, hippocampi were digested in papain solution (20 units of papain per ml in 1 mM L-cysteine with 0.5 mM EDTA) supplemented with DNase I (final concentration 95 units per ml) and shook for 30–60 min at 37°C, 900 rpm. Digested tissue was triturated and set for 3 min, following which the supernatant devoid of tissue chunks was collected. The supernatant was centrifuged at 300x g for 5 min and the pellet was resuspended in resuspension buffer (1 mg of ovomucoid inhibitor, 1 mg of albumin, and 95 units of DNase I per ml in EBSS). The cells were forced to pass through a discontinuous density gradient formed by the resuspension buffer and the Ovomucoid protease inhibitor (10 mg per ml) with bovine serum albumin (10 mg per ml) by centrifuging at 70x g for 6 min. The final cell pellet devoid of membrane fragments was resuspended in Neurobasal-A medium (Gibco, stored at 4 °C) supplemented with Glutamax (Gibco, stored at −20 °C) and B27 (Gibco, stored at −20 °C). Cells were plated on poly-D-lysine coated coverslips mounted on MatTek dishes at a density of 30000-50000 cells/cm[54]. Cultures were maintained at 37°C and 5% CO2 with feeding every 3 days using the same medium until transfection. Transfections were performed 12 days after plating by magnetofection using Combimag (OZ biosciences, stored at 4 °C) and Lipofectamine 2000 (Invitrogen, stored at 4 °C) according to manufacturer's instructions.

**Cell line culture and transfection.**

HeLa and HEK cells were cultured either on poly-ornithine coated glass coverslips or 8 wells ibidis with glass bottom (CliniSciences, 80807-90), in DMEM (Thermo Fisher Scientific, 10566016) supplemented with 10% fetal bovine serum and kept in an incubator with humidified air containing 5% CO2 at a temperature of 37°C. Hela and Hek cells were transfected using Lipofectamine 2000 (Invitrogen), the day before imaging following the Invitrogen recommendations.

**Halo labelling in cells.**

JF dyes were obtained from Dr. Lavis (Janelia Research Campus) or from Promega (HT 1050, Janelia Fluor® 635 HaloTag® Ligand; $JF_{635}$-HTL). The JF dyes obtained from Promega were incubated following the manufacturers instructions. JF dyes obtained from janelia are received at an 100 nmol amount and resuspended in 200 µL DMSO to yield a 500 µM stock. The JF dyes were then diluted in the cell culture media (either DMEM for cell lines or feeding media for primary neuronal cultures) at a final concentration of 1µM. The cells are usually labelled after 30 minutes of incubation but for practical purposes, they were incubated overnight with the dye and the dye was washed in the morning before experiment. To minimize non-specific labeling and reduce background fluorescence, a series of washing steps was performed. The protocol involved replacing the existing media with fresh, pre-warmed culture media, followed by a 10-minute incubation period in a controlled environment. This washing step was repeated twice to ensure thorough removal of non-specific signals and to optimize subsequent fluorescence measurements.

**Calcium imaging, single wavelength recordings.**

Live imaging assays of primary cortical neurons transfected with calcium phosphate method[55] were conducted from DIV12 to DIV21. HEK or HeLa cells imaging assays were performed one day after transfection using lipofectamine 2000 (Thermo Fisher Scientific, 11668019). The experiments utilised a custom-built, laser-illuminated epifluorescence microscope (Zeiss Axio Observer 3) paired with an Andor iXon Life camera (model IXON-L-897), cooled to -70°C. Illumination was provided by fiber-coupled lasers at wavelengths of 488 and 561 nm (Coherent OBIS 488 nm and 561 nm), combined using the Coherent Galaxy Beam Combiner. Laser illumination was controlled by a custom Arduino-based circuit that synchronized imaging and illumination. Neuron-astrocyte co-cultures, HEK or HeLa on coverslips were placed in a closed bath imaging chamber for field stimulation (Warner Instruments, RC-21BRFS) and imaged with a 40x Zeiss oil objective Plan-Neofluar with a numerical aperture of 1.30 (WD = 0.21 mm). Neurons were stimulated using 1 ms current pulses between platinum-iridium electrodes in the stimulating chamber (Warner Instruments, PH-2), driven by a stimulus isolator (WPI, MODEL A382) controlled by the Arduino-based circuit. All the experiments were performed at 37°C. Temperature was kept constant using a Dual Channel Temperature Controller (Warner Instruments, TC-344C) that controlled the temperature of the stimulation chamber (Warner Instruments, PH-2) and simultaneously warmed the imaging solutions using an in-line solution heater (Warner Instruments, SHM-6). Imaging solutions were flown at 0.35-0.40 ml/min. Imaging was performed using a Tyrode's solution composed of (in mM) 119 NaCl, 2.5 KCl, 2 CaCl2, 2 MgCl2 , 20 Glucose together with 10 µM CNQX and 50 µM AP5, buffered to pH 7.4 at 37°C using 25 mM HEPES.

**Calcium imaging in cell lines, multiple wavelengths recordings.**

HeLa or HEK cells expressing two or more calcium sensors were transfected using lipofectamine 2000 (Thermo Fisher Scientific, 11668019) and imaged the next day. Live imaging assays were conducted with an inverted Leica spinning disk equipped with a Yokogawa CSU-X1 module and a Hamamatsu Orca Flash 4.0 sCMOS camera. The objective used was 63x, NA 1.4. Timelapse were acquired with 1.2sec between two images of the same wavelength.

**Image analysis and statistics.**

We used the ImageJ plugin Time Series Analyzer V3 for imaging analysis of dynamic changes in fluorescence. Statistical analysis was carried out using GraphPad Prism v8 for Windows, with specific tests indicated in the Supplementary Table ST1. For each dataset, normality was assessed using Shapiro-Wilk test and then based on the result we chose either parametric or non-parametric tests for further comparisons. All n numbers, as well as the number of independent experiments, are detailed in the Supplementary Table ST1. Unless otherwise indicated, all data for this study was acquired from at least 3 independent experiments. For the figures, the mean and the standard error of mean are used. Results of statistical analysis are shown in figures corresponding to the following criteria: *$p<0.05$, **$p<0.01$, ***$p<0.001$, ****$p < 0.0001$, n.s., not statistically significant.

# Author contributions

Conceptualization, J.d.J-S.; methodology, A.M., H.F., R.F., K.Z., J.d.J.S.; investigation,A.M., H.F., R.F., K.Z., J.d.J.S.; project administration and supervision, J.d.J-S.; writing – original draft, A.M. and J.d.J-S.; writing – review & editing. A.M., H.F., R.F., K.Z., C.G., T.O., V.R., E.S. and J.d.J.S.

# Acknowledgements

We would like to thank all members of the de Juan-Sanz laboratory for insightful discussions and comments. This work was made possible by the Paris Brain Institute Diane Barriere Chair in Synaptic Bioenergetics awarded to J.d.J.-S. Our funding sources are an ERC Starting Grant SynaptoEnergy (European Research Council, ERC-StG-852873), 2019 ATIP-Avenir Grant (CNRS, Inserm), and a Big Brain Theory Grant (ICM) awarded to J.d.J.-S. A.M. is the recipient of a predoctoral fellowship from the French Ministry of Science. J.d.J.-S. is a permanent CNRS researcher and a FENS-Kavli Scholar.

# Declaration of interests

The authors declare no competing interests

# References

1. Berridge, M.J., Lipp, P., and Bootman, M.D. (2000). The versatility and universality of calcium signalling. Nature reviews. Molecular cell biology *1*, 11–21.

https://doi.org/10.1038/35036035.
2. Raffaello, A., Mammucari, C., Gherardi, G., and Rizzuto, R. (2016). Calcium at the center of cell signaling: interplay between endoplasmic reticulum, mitochondria and lysosomes. Trends in biochemical sciences *41*, 1035. https://doi.org/10.1016/J.TIBS.2016.09.001.
3. Mekahli, D., Bultynck, G., Parys, J.B., De Smedt, H., and Missiaen, L. (2011). Endoplasmic-reticulum calcium depletion and disease. Cold Spring Harbor perspectives in biology *3*, a004317-. https://doi.org/10.1101/cshperspect.a004317.
4. Rizzuto, R., De Stefani, D., Raffaello, A., and Mammucari, C. (2012). Mitochondria as sensors and regulators of calcium signalling. Nature reviews. Molecular cell biology *13*, 566–578. https://doi.org/10.1038/nrm3412.
5. Dematteis, G., Tapella, L., Casali, C., Talmon, M., Tonelli, E., Reano, S., Ariotti, A., Pessolano, E., Malecka, J., Chrostek, G., et al. (2024). ER-mitochondria distance is a critical parameter for efficient mitochondrial Ca2+ uptake and oxidative metabolism. Commun Biol *7*, 1–15. https://doi.org/10.1038/s42003-024-06933-9.
6. Liiv, M., Vaarmann, A., Safiulina, D., Choubey, V., Gupta, R., Kuum, M., Janickova, L., Hodurova, Z., Cagalinec, M., Zeb, A., et al. (2024). ER calcium depletion as a key driver for impaired ER-to-mitochondria calcium transfer and mitochondrial dysfunction in Wolfram syndrome. Nat Commun *15*, 6143. https://doi.org/10.1038/s41467-024-50502-x.
7. Lee, K.-S., Huh, S., Lee, S., Wu, Z., Kim, A.-K., Kang, H.-Y., and Lu, B. (2018). Altered ER-mitochondria contact impacts mitochondria calcium homeostasis and contributes to neurodegeneration in vivo in disease models. Proc Natl Acad Sci U S A *115*, E8844–E8853. https://doi.org/10.1073/pnas.1721136115.
8. de Ridder, I., Kerkhofs, M., Lemos, F.O., Loncke, J., Bultynck, G., and Parys, J.B. (2023). The ER-mitochondria interface, where Ca2+ and cell death meet. Cell Calcium *112*, 102743. https://doi.org/10.1016/j.ceca.2023.102743.
9. Loncke, J., Kaasik, A., Bezprozvanny, I., Parys, J.B., Kerkhofs, M., and Bultynck, G. (2021). Balancing ER-Mitochondrial Ca2+ Fluxes in Health and Disease. Trends in Cell Biology *31*, 598–612. https://doi.org/10.1016/j.tcb.2021.02.003.
10. Suzuki, J., Kanemaru, K., Ishii, K., Ohkura, M., Okubo, Y., and Iino, M. (2014). Imaging intraorganellar Ca2+ at subcellular resolution using CEPIA. Nature communications *5*, 4153. https://doi.org/10.1038/ncomms5153.
11. de Juan-Sanz, J., Holt, G.T., Schreiter, E.R., de Juan, F., Kim, D.S., and Ryan, T.A. (2017). Axonal Endoplasmic Reticulum Ca2+ Content Controls Release Probability in CNS Nerve Terminals. Neuron *93*, 867-881.e6. https://doi.org/10.1016/j.neuron.2017.01.010.
12. Bovo, E., Martin, J.L., Tyryfter, J., de Tombe, P.P., and Zima, A.V. (2016). R-CEPIA1er as a new tool to directly measure sarcoplasmic reticulum [Ca] in ventricular myocytes. Am J Physiol Heart Circ Physiol *311*, H268–H275. https://doi.org/10.1152/ajpheart.00175.2016.
13. Ashrafi, G., de Juan-Sanz, J., Farrell, R.J., and Ryan, T.A. (2020). Molecular Tuning of the Axonal Mitochondrial Ca2+ Uniporter Ensures Metabolic Flexibility of Neurotransmission. Neuron *105*, 678-687.e5. https://doi.org/10.1016/j.neuron.2019.11.020.
14. Wu, J., Prole, D.L., Shen, Y., Lin, Z., Gnanasekaran, A., Liu, Y., Chen, L., Zhou, H., Chen, S.R.W., Usachev, Y.M., et al. (2014). Red fluorescent genetically encoded Ca 2+ indicators for use in mitochondria and endoplasmic reticulum. Biochemical Journal *464*, 13–22. https://doi.org/10.1042/BJ20140931.
15. Henderson, M.J., Baldwin, H.A., Werley, C.A., Boccardo, S., Whitaker, L.R., Yan, X., Holt, G.T., Schreiter, E.R., Looger, L.L., Cohen, A.E., et al. (2015). A Low Affinity GCaMP3

Variant (GCaMPer) for Imaging the Endoplasmic Reticulum Calcium Store. PloS one *10*, e0139273. https://doi.org/10.1371/journal.pone.0139273.
16. Okubo, Y., Suzuki, J., Kanemaru, K., Nakamura, N., Shibata, T., and Iino, M. (2015). Visualization of Ca2+ Filling Mechanisms upon Synaptic Inputs in the Endoplasmic Reticulum of Cerebellar Purkinje Cells. The Journal of neuroscience : the official journal of the Society for Neuroscience *35*, 15837–15846. https://doi.org/10.1523/JNEUROSCI.3487-15.2015.
17. Hirabayashi, Y., Kwon, S.K., Paek, H., Pernice, W.M., Paul, M.A., Lee, J., Erfani, P., Raczkowski, A., Petrey, D.S., Pon, L.A., et al. (2017). ER-mitochondria tethering by PDZD8 regulates Ca2+ dynamics in mammalian neurons. Science *358*, 623–630. https://doi.org/10.1126/science.aan6009.
18. Kwon, S.K., Sando, R., Lewis, T.L., Hirabayashi, Y., Maximov, A., and Polleux, F. (2016). LKB1 Regulates Mitochondria-Dependent Presynaptic Calcium Clearance and Neurotransmitter Release Properties at Excitatory Synapses along Cortical Axons. PLOS Biology *14*, e1002516. https://doi.org/10.1371/JOURNAL.PBIO.1002516.
19. Vaccaro, V., Devine, M.J., Higgs, N.F., and Kittler, J.T. (2017). Miro1-dependent mitochondrial positioning drives the rescaling of presynaptic Ca2+ signals during homeostatic plasticity. EMBO reports *18*, 231–240. https://doi.org/10.15252/EMBR.201642710.
20. Deo, C., Abdelfattah, A.S., Bhargava, H.K., Berro, A.J., Falco, N., Farrants, H., Moeyaert, B., Chupanova, M., Lavis, L.D., and Schreiter, E.R. (2021). The HaloTag as a general scaffold for far-red tunable chemigenetic indicators. Nature Chemical Biology *17*. https://doi.org/10.1038/s41589-021-00775-w.
21. Farrell, R.J., Bredvik, K.G., Hoppa, M.B., Hennigan, S.T., Brown, T.A., and Ryan, T.A. (2024). A ratiometric ER calcium sensor for quantitative comparisons across cell types and subcellular regions. bioRxiv, 02.15.580492. https://doi.org/10.1101/2024.02.15.580492.
22. Courjaret, R., Dib, M., and Machaca, K. (2018). Spatially restricted subcellular Ca2+ signaling downstream of store-operated calcium entry encoded by a cortical tunneling mechanism. Sci Rep *8*, 11214. https://doi.org/10.1038/s41598-018-29562-9.
23. Terasaki, M. (2018). Axonal endoplasmic reticulum is very narrow. Journal of cell science *131*, jcs210450. https://doi.org/10.1242/jcs.210450.
24. Wu, Y., Whiteus, C., Xu, C.S., Hayworth, K.J., Weinberg, R.J., Hess, H.F., and De Camilli, P. (2017). Contacts between the endoplasmic reticulum and other membranes in neurons. Proceedings of the National Academy of Sciences of the United States of America *114*, E4859–E4867. https://doi.org/10.1073/pnas.1701078114.
25. Spacek, J., and Harris, K.M. (1997). Three-Dimensional Organization of Smooth Endoplasmic Reticulum in Hippocampal CA1 Dendrites and Dendritic Spines of the Immature and Mature Rat. J. Neurosci. *17*, 190–203. https://doi.org/10.1523/JNEUROSCI.17-01-00190.1997.
26. Panzera, L.C., Johnson, B., Quinn, J.A., Cho, I.H., Tamkun, M.M., and Hoppa, M.B. (2022). Activity-dependent endoplasmic reticulum Ca2+ uptake depends on Kv2.1-mediated endoplasmic reticulum/plasma membrane junctions to promote synaptic transmission. Proceedings of the National Academy of Sciences *119*, e2117135119. https://doi.org/10.1073/pnas.2117135119.
27. Oliva, M.K., Pérez-Moreno, J.J., O'Shaughnessy, J., Wardill, T.J., and O'Kane, C.J. (2020). Endoplasmic Reticulum Lumenal Indicators in Drosophila Reveal Effects of HSP-Related

Mutations on Endoplasmic Reticulum Calcium Dynamics. Frontiers in Neuroscience *14*, 816. https://doi.org/10.3389/fnins.2020.00816.
28. Grieves, R.M., Wood, E.R., and Dudchenko, P.A. (2016). Place cells on a maze encode routes rather than destinations. eLife *5*. https://doi.org/10.7554/ELIFE.15986.
29. Benedetti, L., Fan, R., Weigel, A.V., Moore, A.S., Houlihan, P.R., Kittisopikul, M., Park, G., Petruncio, A., Hubbard, P.M., Pang, S., et al. (2024). Periodic ER-plasma membrane junctions support long-range Ca2+ signal integration in dendrites. Preprint at bioRxiv, https://doi.org/10.1101/2024.05.27.596121 https://doi.org/10.1101/2024.05.27.596121.
30. Zhou, Z., Matlib, M.A., and Bers, D.M. (1998). Cytosolic and mitochondrial Ca2+ signals in patch clamped mammalian ventricular myocytes. J Physiol *507 ( Pt 2)*, 379–403. https://doi.org/10.1111/j.1469-7793.1998.379bt.x.
31. Di Lisa, F., Gambassi, G., Spurgeon, H., and Hansford, R.G. (1993). Intramitochondrial free calcium in cardiac myocytes in relation to dehydrogenase activation. Cardiovasc Res *27*, 1840–1844. https://doi.org/10.1093/cvr/27.10.1840.
32. Miyata, H., Silverman, H.S., Sollott, S.J., Lakatta, E.G., Stern, M.D., and Hansford, R.G. (1991). Measurement of mitochondrial free Ca2+ concentration in living single rat cardiac myocytes. Am J Physiol *261*, H1123-1134. https://doi.org/10.1152/ajpheart.1991.261.4.H1123.
33. Groten, C.J., and MacVicar, B.A. (2022). Mitochondrial Ca2+ uptake by the MCU facilitates pyramidal neuron excitability and metabolism during action potential firing. Commun Biol *5*, 1–15. https://doi.org/10.1038/s42003-022-03848-1.
34. Bredvik, K., and Ryan, T.A. (2024). Differential Control of Inhibitory and Excitatory Nerve Terminal Function by Mitochondria. Preprint at bioRxiv, https://doi.org/10.1101/2024.05.19.594864 https://doi.org/10.1101/2024.05.19.594864.
35. Kar, P., Samanta, K., and Parekh, A.B. (2020). Cytosolic and intra-organellar Ca2+ oscillations: mechanisms and function. Current Opinion in Physiology *17*, 175–186. https://doi.org/10.1016/j.cophys.2020.08.011.
36. Zheng, S., Wang, X., Zhao, D., Liu, H., and Hu, Y. (2023). Calcium homeostasis and cancer: insights from endoplasmic reticulum-centered organelle communications. Trends in Cell Biology *33*, 312–323. https://doi.org/10.1016/j.tcb.2022.07.004.
37. Si, H., Wang, J., Meininger, C.J., Peng, X., Zawieja, D.C., and Zhang, S.L. (2020). Ca2+ release-activated Ca2+ channels are responsible for histamine-induced Ca2+ entry, permeability increase, and interleukin synthesis in lymphatic endothelial cells. American Journal of Physiology-Heart and Circulatory Physiology *318*, H1283–H1295. https://doi.org/10.1152/ajpheart.00544.2019.
38. Cartes-Saavedra, B., Macuada, J., Lagos, D., Arancibia, D., Andrés, M.E., Yu-Wai-Man, P., Hajnóczky, G., and Eisner, V. (2022). OPA1 Modulates Mitochondrial Ca2+ Uptake Through ER-Mitochondria Coupling. Front Cell Dev Biol *9*, 774108. https://doi.org/10.3389/fcell.2021.774108.
39. Lopez-Crisosto, C., Díaz-Vegas, A., Castro, P.F., Rothermel, B.A., Bravo-Sagua, R., and Lavandero, S. (2021). Endoplasmic reticulum−mitochondria coupling increases during doxycycline-induced mitochondrial stress in HeLa cells. Cell Death Dis *12*, 1–12. https://doi.org/10.1038/s41419-021-03945-9.
40. Farrants, H., Shuai, Y., Lemon, W.C., Monroy Hernandez, C., Zhang, D., Yang, S., Patel, R., Qiao, G., Frei, M.S., Plutkis, S.E., et al. (2024). A modular chemigenetic calcium indicator for multiplexed in vivo functional imaging. Nat Methods *21*, 1916–1925.

https://doi.org/10.1038/s41592-024-02411-6.
41. Abdelfattah, A.S., Kawashima, T., Singh, A., Novak, O., Liu, H., Shuai, Y., Huang, Y.-C., Campagnola, L., Seeman, S.C., Yu, J., et al. (2019). Bright and photostable chemigenetic indicators for extended in vivo voltage imaging. Science *365*, 699–704. https://doi.org/10.1126/science.aav6416.
42. Abdelfattah, A.S., Valenti, R., Zheng, J., Wong, A., GENIE Project Team, Podgorski, K., Koyama, M., Kim, D.S., and Schreiter, E.R. (2020). A general approach to engineer positive-going eFRET voltage indicators. Nat Commun *11*, 3444. https://doi.org/10.1038/s41467-020-17322-1.
43. Hellweg, L., Edenhofer, A., Barck, L., Huppertz, M.-C., Frei, M.S., Tarnawski, M., Bergner, A., Koch, B., Johnsson, K., and Hiblot, J. (2023). A general method for the development of multicolor biosensors with large dynamic ranges. Nat Chem Biol *19*, 1147–1157. https://doi.org/10.1038/s41589-023-01350-1.
44. Asanuma, D., Takaoka, Y., Namiki, S., Takikawa, K., Kamiya, M., Nagano, T., Urano, Y., and Hirose, K. (2014). Acidic-pH-activatable fluorescence probes for visualizing exocytosis dynamics. Angew Chem Int Ed Engl *53*, 6085–6089. https://doi.org/10.1002/anie.201402030.
45. Liu, Y., Miao, K., Li, Y., Fares, M., Chen, S., and Zhang, X. (2018). A HaloTag-Based Multicolor Fluorogenic Sensor Visualizes and Quantifies Proteome Stress in Live Cells Using Solvatochromic and Molecular Rotor-Based Fluorophores. Biochemistry *57*, 4663–4674. https://doi.org/10.1021/acs.biochem.8b00135.
46. Cook, A., Walterspiel, F., and Deo, C. (2023). HaloTag-Based Reporters for Fluorescence Imaging and Biosensing. ChemBioChem *24*, e202300022. https://doi.org/10.1002/cbic.202300022.
47. Farrants, H., Hiblot, J., Griss, R., and Johnsson, K. (2017). Rational Design and Applications of Semisynthetic Modular Biosensors: SNIFITs and LUCIDs. Methods Mol Biol *1596*, 101–117. https://doi.org/10.1007/978-1-4939-6940-1_7.
48. Deo, C., Sheu, S.-H., Seo, J., Clapham, D.E., and Lavis, L.D. (2019). Isomeric Tuning Yields Bright and Targetable Red Ca2+ Indicators. J Am Chem Soc *141*, 13734–13738. https://doi.org/10.1021/jacs.9b06092.
49. Mertes, N., Busch, M., Huppertz, M.-C., Hacker, C.N., Wilhelm, J., Gürth, C.-M., Kühn, S., Hiblot, J., Koch, B., and Johnsson, K. (2022). Fluorescent and Bioluminescent Calcium Indicators with Tuneable Colors and Affinities. J Am Chem Soc *144*, 6928–6935. https://doi.org/10.1021/jacs.2c01465.
50. Patron, M., Granatiero, V., Espino, J., Rizzuto, R., and De Stefani, D. (2018). MICU3 is a tissue-specific enhancer of mitochondrial calcium uptake. Cell Death & Differentiation. https://doi.org/10.1038/s41418-018-0113-8.
51. Gottschalk, B., Koshenov, Z., Waldeck-Weiermair, M., Radulović, S., Oflaz, F.E., Hirtl, M., Bachkoenig, O.A., Leitinger, G., Malli, R., and Graier, W.F. (2022). MICU1 controls spatial membrane potential gradients and guides Ca2+ fluxes within mitochondrial substructures. Commun Biol *5*, 1–13. https://doi.org/10.1038/s42003-022-03606-3.
52. Studier, F.W. (2005). Protein production by auto-induction in high-density shaking cultures. Protein Expression and Purification *41*, 207–234. https://doi.org/10.1016/j.pep.2005.01.016.
53. Tsien, R., and Pozzan, T. (1989). Measurement of cytosolic free Ca2+ with quin2. Methods Enzymol *172*, 230–262. https://doi.org/10.1016/s0076-6879(89)72017-6.
54. Vishwanath, A.A., Comyn, T., Chintaluri, C., Ramon-Duaso, C., Fan, R., Sivakumar, R.,

Lopez-Manzaneda, M., Preat, T., Vogels, T.P., Rangaraju, V., et al. (2024). Mitochondrial Ca2+ efflux controls neuronal metabolism and long-term memory across species. Preprint at bioRxiv, https://doi.org/10.1101/2024.02.01.578153 https://doi.org/10.1101/2024.02.01.578153.

55. Cuhadar, U., Calzado-Reyes, L., Pascual-Caro, C., Aberra, A.S., Ritzau-Jost, A., Aggarwal, A., Ibata, K., Podgorski, K., Yuzaki, M., Geis, C., et al. (2024). Activity-driven synaptic translocation of LGI1 controls excitatory neurotransmission. Cell Reports *43*. https://doi.org/10.1016/j.celrep.2024.114186.

# Figure legends

**Figure 1. ER-HaloCaMP$_{585}$ is a bright and highly responsive red ER $Ca^{2+}$ sensor.**
**(A)** Predicted structure of low affinity HaloCaMP showing the mutations in the CaM domain in blue, $Ca^{2+}$ binding sites in yellow and the binding of JF$_{585}$-HTL in red. The HaloTag is represented in grey. **(B)** Screening for low affinity HaloCaMP variants: *in vitro* $Ca^{2+}$ titrations of different purified HaloCaMP variants conjugated with JF$_{585}$-HTL. **(C)** Top: targeting scheme for expression in the ER by adding the N-terminal signal peptide of calreticulin (CALR sig peptide) and the C-terminal KDEL retention motif. Bottom: high resolution image of a Hela cell expressing ER-localized LA-HaloCaMP reconstituted with JF$_{585}$-HTL shows the ER structure. Pseudocolor scale shows low to high fluorescence intensity. Scale bar, 1.03 µm. **(D)** Predicted responsiveness versus $Ca^{2+}$ curves based on binding parameters of ER-HaloCaMP$_{585}$, LAR-GECO1 and R-CEPIAer. **(E)** Quantification of thapsigargin response (1 µM) in both Hela cells and cortical neuron somas. **(F-H)** Comparison of relative brightness of LAR-GECO, R-CEPIAer and ER-HaloCaMP$_{585}$ using identical illumination and detection conditions in either Hela cells or cortical neurons. **(F)** Quantification of sensor brightness in intact Hela cells or cortical neuron somas. **(G)** Representative images of brightness level in neuronal soma. Scale bar, 9.27, µm **(H)** Quantification of the ability of red ER calcium sensors to detect single ER tubules of axons. Data are represented as mean ± SEM. See Supplementary Table ST1 for details on statistical tests and sample sizes.

**Figure 2. ER-HaloCaMP$_{585}$ enables ER $Ca^{2+}$ measurements in subcellular locales with low ER content.**
**(A-D)** Axonal ER $Ca^{2+}$ responses to 20 AP (20 Hz) stimulation, using different indicators. **(A)** On the left: schematic representation of ER-HaloCaMP$_{585}$ expressed within a single ER tubule of axon. On the right representative image of a neuron expressing ER-HaloCaMP$_{585}$, zoomed on an axon. Scale bar, 4 µm. Corresponding kymograph (pseudocolor scale below showing low to high intensity). **(B)** Corresponding fluorescence intensity over time, before and after thapsigargin treatment (1 µM). **(C)** Quantification of activity-driven ER $Ca^{2+}$ uptake peak response upon 20 AP (20 Hz) stimulation. **(D)** Quantification of relative brightness measured with ER-GCaMP-210 or ER-HaloCaMP$_{585}$ in axons. **(E-H)** Dendritic ER $Ca^{2+}$ responses to glutamate uncaging in spines. **(E)** On the left: schematic representation of ER-HaloCaMP$_{585}$ expressed within the dendritic compartment. On the right representative image of a neuron expressing ER-HaloCaMP$_{585}$, zoomed in the dendritic compartment (pseudocolor scale below showing low to high intensity). Scale bar, 4 µm. **(F)** Corresponding fluorescence intensity over time, measured with ER-HaloCaMP$_{585}$ or ER-GCaMP-210. **(G)** Quantification of the ER $Ca^{2+}$ peak release. **(H)** Corresponding quantification of fluorescence recovery. Data are represented as mean ± SEM. See Supplementary Table ST1 for details on statistical tests and sample sizes.

**Figure 3. Far red ER Ca2+ measurements using ER-HaloCaMP$_{635}$.**
**(A)** High resolution image of a Hela cell expressing ER-HaloCaMP1a reconstituted with JF$_{635}$-HTL shows the ER structure (pseudocolor scale below showing low to high intensity). Scale bar, 12.36 µm. **(B)** Average fluorescence intensity over time, upon thapsigargin treatment (1 µM) in Hela cells, measured with ER-HaloCaMP$_{635}$. **(C)** Quantification of the thapsigargin response (1 µM) in Hela cells, measured with different sensors. **(D-F)** Axonal ER $Ca^{2+}$ responses to 20 AP (20 Hz) stimulation, using different indicators. **(D)** On the left: schematic representation of ER-HaloCaMP$_{635}$ expressed within a single ER tubule of axon. On the right representative image of a neuron expressing ER-HaloCaMP$_{635}$, zoomed on an axon. Scale bar, 4 µm. Corresponding kymograph (pseudocolor scale below showing low to high intensity). **(E)** Corresponding fluorescence intensity over time, before and after thapsigargin treatment (1 µM). **(F)** Quantification of activity-driven ER $Ca^{2+}$ uptake peak response upon 20 AP (20 Hz) stimulation. Data are represented as mean ± SEM. See Supplementary Table ST1 for details on statistical tests and sample sizes.

**Figure 4. Mito-HaloCaMP is a tunable and highly responsive mitochondrial $Ca^{2+}$ sensor.**
**(A)** Top: targeting scheme for expression in the mitochondria by adding 4 times COX8 mitochondrial targeting sequence (MTS). Bottom: high resolution image of a Hela cell expressing Mito-HaloCaMP reconstituted with JF$_{585}$-HTL shows the mitochondrial structures (pseudocolor scale below showing low to high intensity). Scale bar, 2.06 µm. **(B)** Average fluorescence intensity over time, upon histamine treatment (10 µM), measured with red mitochondrial calcium indicators in Hela cells. **(C)** Corresponding quantification of the peak response. **(D)** Comparison of relative brightness of mito-RCaMP1b and mito-HaloCaMP$_{585}$ using identical illumination and detection conditions in intact Hela cells. **(E)** On the left: schematic representation of mito-HaloCaMP$_{585}$ expressed within a single ER tubule of axon. On the right representative image of a neuron expressing mito-HaloCaMP$_{585}$, zoomed on an axon. Scale bar, 4 µm. Corresponding kymograph (pseudocolor scale below showing low to high intensity). **(F)** Corresponding average fluorescence intensity over time upon 20 AP (20 Hz) stimulation, measured with red mitochondrial calcium indicators in axons of cortical neurons. **(G)** Quantification of activity-driven mitochondrial $Ca^{2+}$ uptake peak response upon 20 AP (20 Hz) stimulation or 100 AP (100 Hz) with red mitochondrial calcium indicators. **(H)** High resolution image of a Hela cell expressing Mito-HaloCaMP reconstituted with JF$_{635}$-HTL (pseudocolor scale below showing low to high intensity). Scale bar, 2.06 µm. **(I-K)** Simultaneous expression of mito-HaloCaMP$_{585,}$ jRCaMP1b and ER-GCaMP-210 in Hela cells. **(I)** Single cell recording of mitochondria, cytosolic and ER $Ca^{2+}$ upon ATP (100 µM) application. **(J)** Corresponding correlation study between peak response of ER, cytosolic and mitochondria during ATP application. **(K)** Quantification of ER-mitochondrial $Ca^{2+}$ transfer during 10 µM histamine addition. ER, mitochondria and cytosol peak responses obtained in single cells were processed to obtain their coupling factor: Mitochondrial $Ca^{2+}$ peak / (Mitochondrial $Ca^{2+}$ peak + Cytosolic $Ca^{2+}$ peak). Single-cell coupling factor data were grouped using a binning size of 0.2 and corresponding ER $Ca^{2+}$ peak for each bin was averaged and plotted in the y-axis. Line shows fitting to a single-exponential curve. **(L-O)** Axonal mitochondrial $Ca^{2+}$ responses to 20 AP (20 Hz) and 100 AP (100 Hz) stimulation, using Mito-HaloCaMP reconstituted with JF$_{635}$-HTL. **(L)** On the left: schematic representation of mito-HaloCaMP$_{635}$ expressed within a single ER tubule of axon. On the right representative image of a neuron expressing mito-HaloCaMP$_{635}$, zoomed on an axon. Scale bar, 4 µm. Corresponding kymograph (pseudocolor scale below showing low to high intensity). **(M)** Average fluorescence intensity over time upon 20 AP (20 Hz) stimulation. **(N)** Average fluorescence intensity over time upon 100 AP (100 Hz) stimulation. **(O)** Quantification of activity-driven mitochondrial $Ca^{2+}$ uptake peak response upon 100 AP (100 Hz)

measured with Mito-GCaMP6f and mito-HaloCaMP$_{635}$. Data are represented as mean ± SEM. See Supplementary Table ST1 for details on statistical tests and sample sizes.

**Supp. Fig. S1. Biochemical properties of LA-HaloCaMP1.**
**(A)** Predicted structure of low affinity HaloCaMP vs HaloTagCPY, composed of HaloTag (PDBID = 6Y7B) and CaM-peptide (PDBID = 1CDL). **(B)** Comparative measurements of responsiveness and affinity in purified LA-HaloCaMP1a$_{585}$ both at room temperature (RT) and at 37°C. **(C)** In-cell calibration at 37°C of ER-HaloCaMP$_{585}$ expressed in permeabilized HeLa cells. Signals are normalized to mTagBFP2 fluorescence in each cell measured. Data are represented as mean ± SEM. See Supplementary Table ST1 for details on sample sizes.

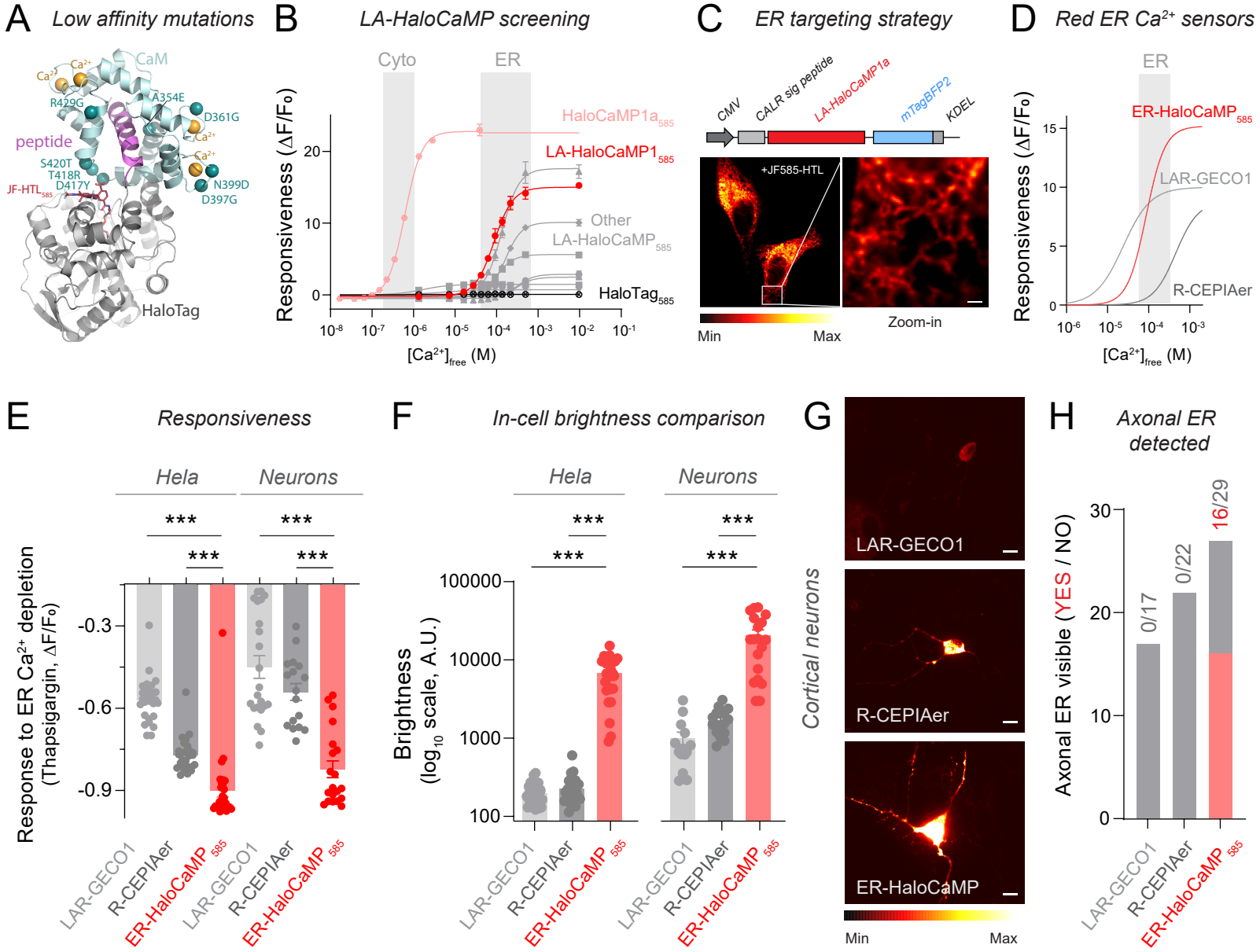
A
Low affinity mutations
CaM
Ca2+
R429G
A354E
D361G
peptide
S420T
T418R
D417Y
JF-HTL585
N399D
D397G
HaloTag
B
LA-HaloCaMP screening
Cyto
ER
HaloCaMP1a585
LA-HaloCaMP1585
Other
LA-HaloCaMP585
HaloTag585
Responsiveness (ΔF/F0)
[Ca2+]free (M)
C
ER targeting strategy
CMV
CALR sig peptide
LA-HaloCaMP1a
mTagBFP2
KDEL
+JF585-HTL
Min
Max
Zoom-in
D
Red ER Ca2+ sensors
ER
ER-HaloCaMP585
LAR-GECO1
R-CEPIAer
Responsiveness (ΔF/F0)
[Ca2+]free (M)
E
Responsiveness
Hela
Neurons
Response to ER Ca2+ depletion (Thapsigargin, ΔF/F0)
LAR-GECO1
R-CEPIAer
ER-HaloCaMP585
F
In-cell brightness comparison
Hela
Neurons
Brightness (log10 scale, A.U.)
G
Cortical neurons
LAR-GECO1
R-CEPIAer
ER-HaloCaMP
Min
Max
H
Axonal ER detected
Axonal ER visible (YES / NO)
0/17
0/22
16/29

FIGURE 1

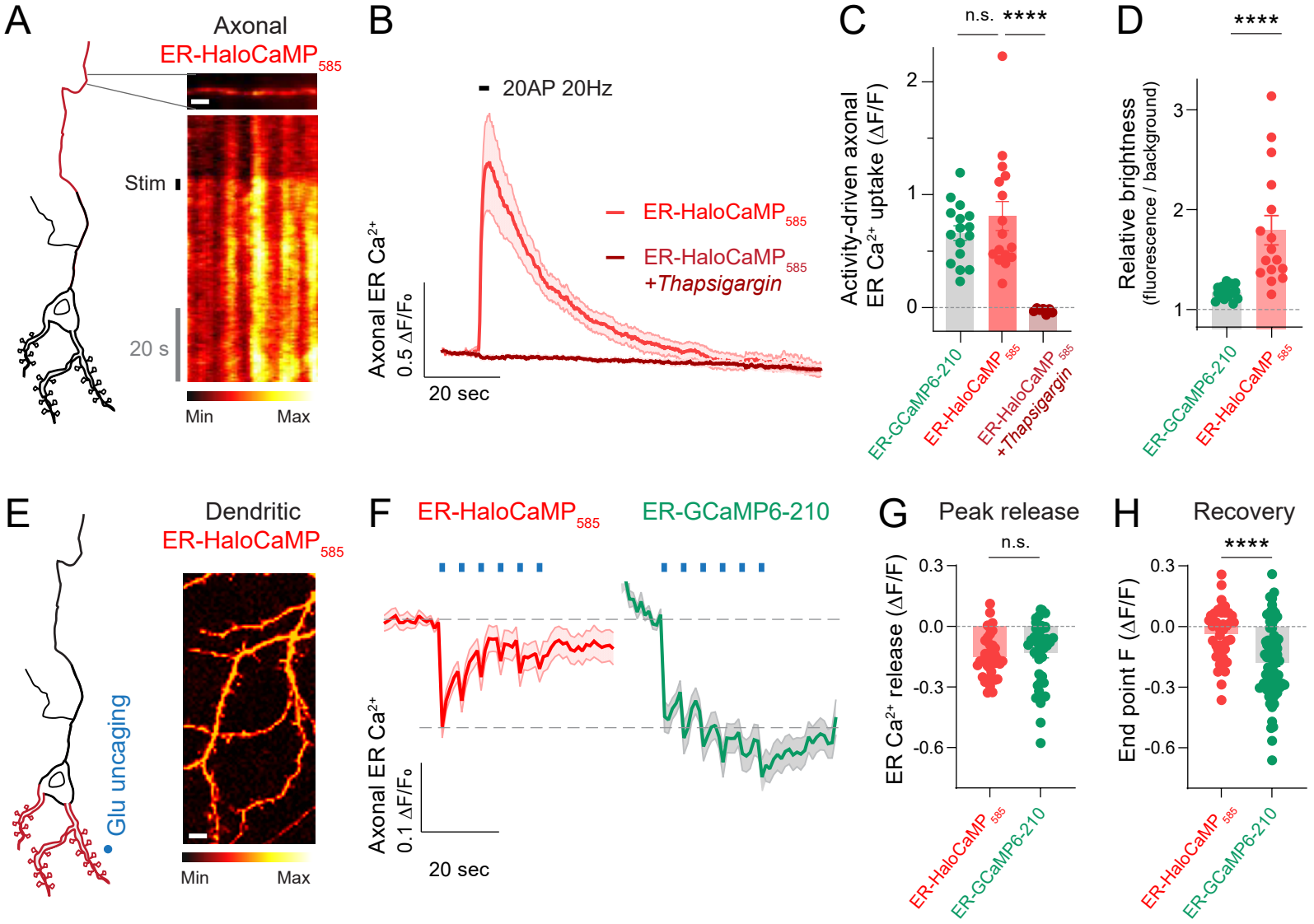
A
Axonal
ER-HaloCaMP585
Stim
20 s
Min
Max
B
20AP 20Hz
ER-HaloCaMP585
ER-HaloCaMP585
+Thapsigargin
Axonal ER Ca2+
0.5 ΔF/F0
20 sec
C
n.s.
****
Activity-driven axonal
ER Ca2+ uptake (ΔF/F)
ER-GCaMP6-210
ER-HaloCaMP585
ER-HaloCaMP585
+Thapsigargin
D
****
Relative brightness
(fluorescence / background)
ER-GCaMP6-210
ER-HaloCaMP585
E
Dendritic
ER-HaloCaMP585
Glu uncaging
Min
Max
F
ER-HaloCaMP585
ER-GCaMP6-210
Axonal ER Ca2+
0.1 ΔF/F0
20 sec
G
Peak release
n.s.
ER Ca2+ release (ΔF/F)
ER-HaloCaMP585
ER-GCaMP6-210
H
Recovery
****
End point F (ΔF/F)
ER-HaloCaMP585
ER-GCaMP6-210

*FIGURE 2*

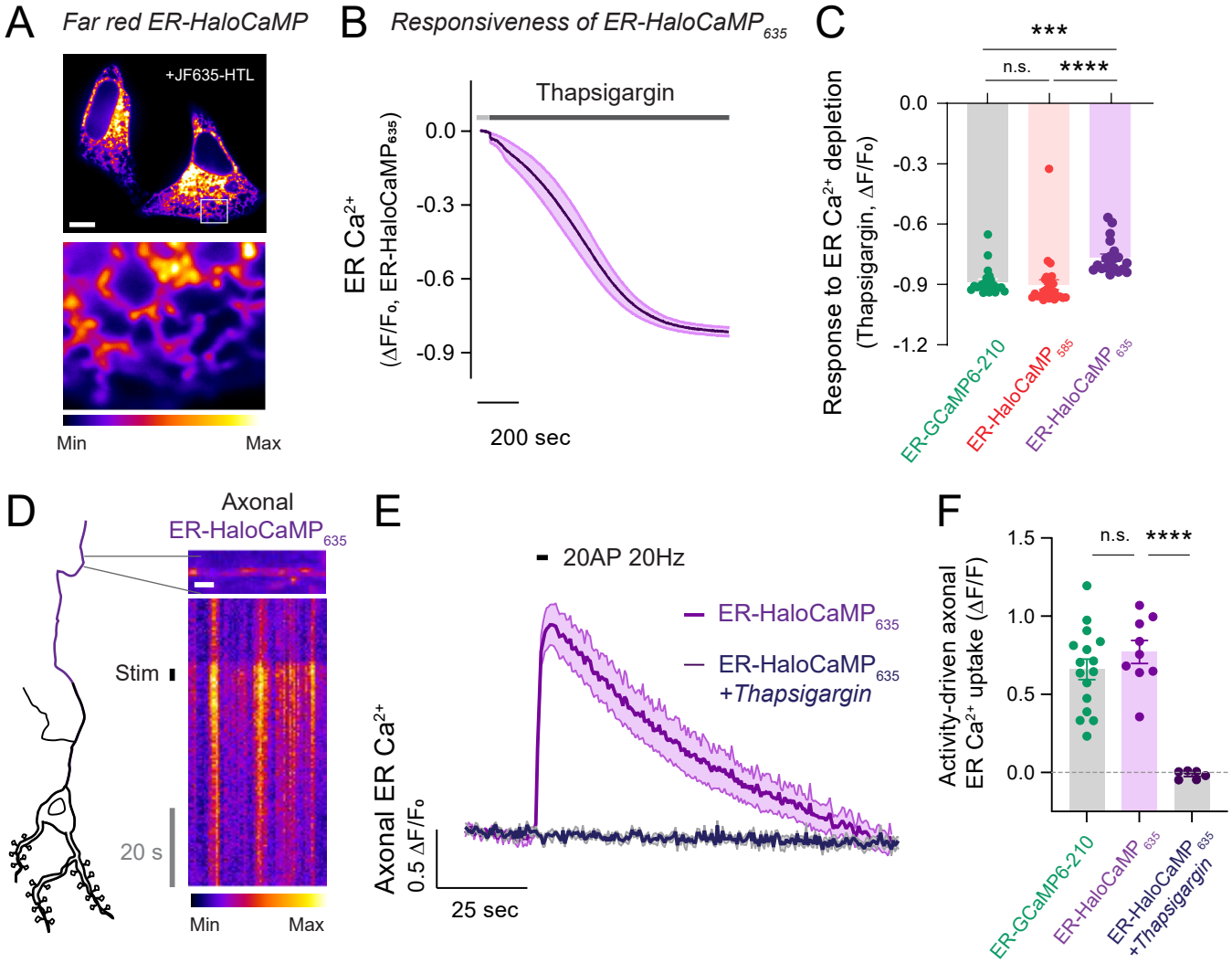
A
Far red ER-HaloCaMP
+JF635-HTL
Min
Max
B
Responsiveness of ER-HaloCaMP635
Thapsigargin
ER Ca2+
(ΔF/Fo, ER-HaloCaMP635)
0.0
-0.3
-0.6
-0.9
200 sec
C
***
n.s.
****
Response to ER Ca2+ depletion
(Thapsigargin, ΔF/Fo)
0.0
-0.3
-0.6
-0.9
-1.2
ER-GCaMP6-210
ER-HaloCaMP585
ER-HaloCaMP635
D
Axonal
ER-HaloCaMP635
Stim
20 s
Min
Max
E
20AP 20Hz
ER-HaloCaMP635
ER-HaloCaMP635
+Thapsigargin
Axonal ER Ca2+
0.5 ΔF/Fo
25 sec
F
n.s.
****
Activity-driven axonal
ER Ca2+ uptake (ΔF/F)
1.5
1.0
0.5
0.0
ER-GCaMP6-210
ER-HaloCaMP635
ER-HaloCaMP635
+Thapsigargin

*FIGURE 3*

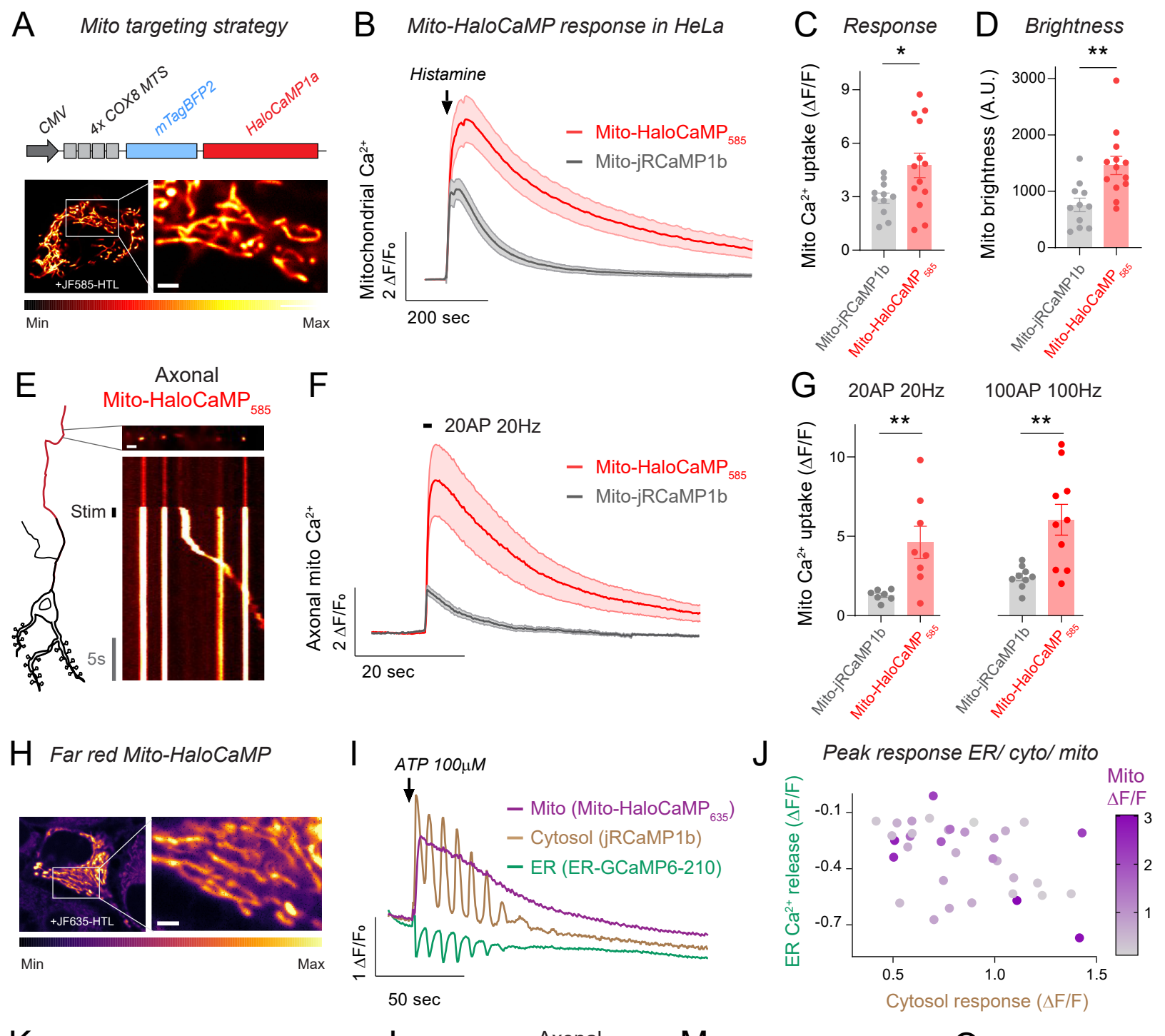
A
Mito targeting strategy
CMV
4x COX8 MTS
mTagBFP2
HaloCaMP1a
+JF585-HTL
Min
Max
B
Mito-HaloCaMP response in HeLa
Histamine
Mito-HaloCaMP585
Mito-jRCaMP1b
Mitochondrial Ca2+
2 ΔF/Fo
200 sec
C
Response
Mito Ca2+ uptake (ΔF/F)
Mito-jRCaMP1b
Mito-HaloCaMP 585
D
Brightness
Mito brightness (A.U.)
E
Axonal
Mito-HaloCaMP585
Stim
5s
F
20AP 20Hz
Axonal mito Ca2+
20 sec
G
20AP 20Hz
100AP 100Hz
H
Far red Mito-HaloCaMP
+JF635-HTL
I
ATP 100μM
Mito (Mito-HaloCaMP635)
Cytosol (jRCaMP1b)
ER (ER-GCaMP6-210)
1 ΔF/Fo
50 sec
J
Peak response ER/ cyto/ mito
ER Ca2+ release (ΔF/F)
Cytosol response (ΔF/F)
Mito ΔF/F
K
ER-mitochondria Ca2+ coupling
Coupling factor
Mito / (Mito + Cyto)
Balanced
More Cyto Ca2+
More Mito Ca2+
L
Axonal
Mito-HaloCaMP635
M
20AP 20Hz
0.5 ΔF/Fo
25 sec
N
100AP 100Hz
O
Mito Ca2+ uptake (100AP 100Hz, ΔF/F)
Mito-HaloCaMP 635
Mito-GCaMP6f

FIGURE 4

A

*Predicted structure of LA-HaloCaMP vs HaloTagCPY*

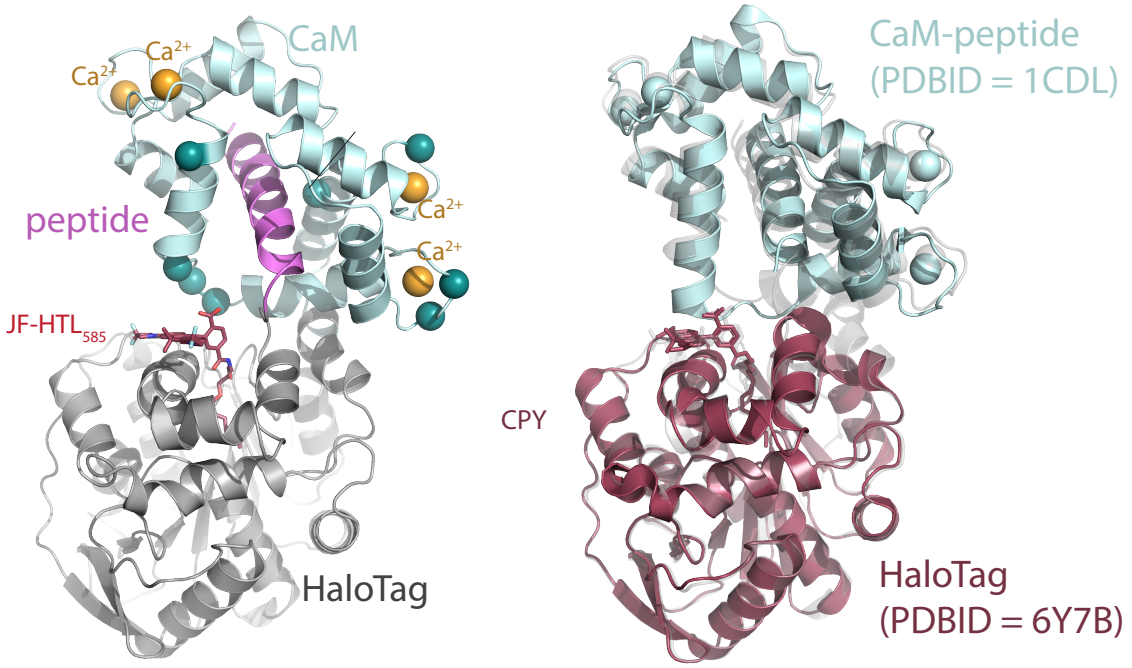


B

*Purified protein, LA-HaloCaMP1a585*

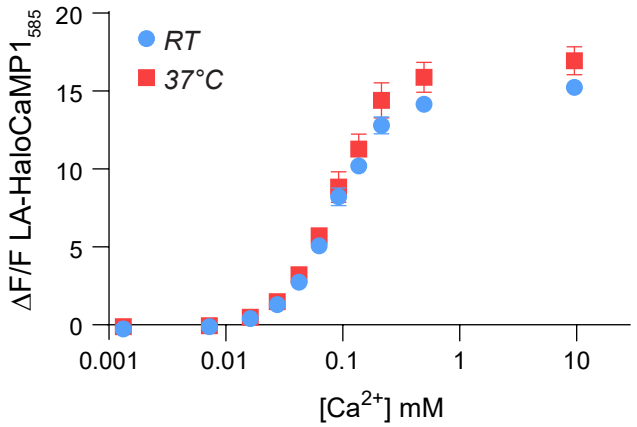


C

*In-cell calibration, 37°C, LA-HaloCaMP1a585*

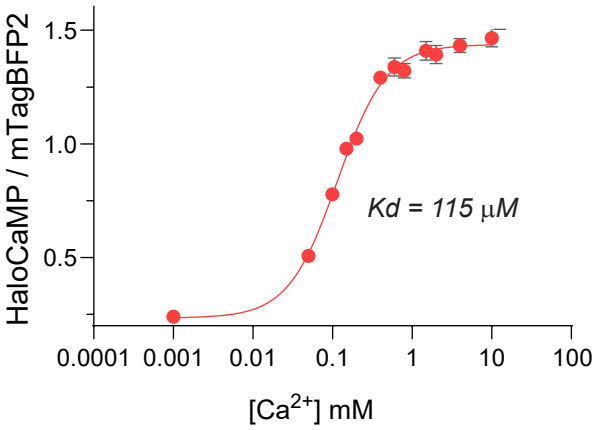


*SUPP. FIGURE 1*